



Predicting spatial patterns of within-field crop yield variability

Bernardo Maestrini, Bruno Basso*

Department of Earth and Environmental Sciences, Michigan State University, East Lansing, 48823, MI, USA



ARTICLE INFO

Keywords:

Yield map
NDVI
Aerial images
Plant surface temperature
Management zones
Precision agriculture

ABSTRACT

Over the last two decades, there has been significant advancements in the application of geospatial technologies in agriculture. Improved resolutions (spectral, spatial and temporal) of remotely sensed images, coupled with more precise on-the-ground systems (yield monitors, geophysical sensors) have allowed farmers to become more sensitive about the spatial and temporal variations of crop yields occurring in their fields. Previous research has extensively looked at spatial variability of crop yields at field scale, but studies designed to predict within-field spatial patterns of yield over a large number of fields as yet been reported. In this paper, we analyzed 571 fields with multiple years of yield maps at high spatial resolution to understand and predict within-field spatial patterns across eight states in the Midwest US and over corn, soybean, wheat and cotton fields. We examined the correlation between yield and 4 covariates, three derived from remote sensing imagery (red band spectral reflectance, NDVI and plant surface temperature) and the fourth from yield maps from previous years. The results showed that for spatial patterns that are stable over time the best predictor of the spatial variability is the historical yield map (previous years' yield maps), while for zones within the field that are more sensitive to weather and thus fluctuate from one year to the next the best predictor of the spatial patterns are the within-season images. The results of this research help quantify the role of historical yield maps and within-season remote sensing images to predict spatial patterns. The knowledge of spatial patterns within a field is critical not only to farmers for potential variable rate applications, but also to select homogenous zones within the field to run crop models with site-specific input to better understand and predict the impact of weather, soil and landscape characteristics on spatial and temporal patterns of crop yields to enhance resource use efficiency at field level.

1. Introduction

In order to apply variable rate input within a field (Schepers et al., 2004), it is essential to understand the drivers of the spatial distribution of yield at field scale. A number of studies have investigated the determinants of spatial variability of yield at the level of a single field (Basso et al., 2011; Koshla et al., 2010) however few studies have attempted to compare predictors of yield spatial patterns over a large number of fields.

Here we investigate factors that predict within-field yield spatial variability by dividing fields into stable and unstable portions, based on the yield temporal variability that each point of the field exhibits over three or more growing seasons (Basso et al., 2007; Blackmore, 2000). In the stable portions of a field, the main determinants of spatial distribution of yield are related to soil properties and landscape position. However, in areas where yield is unstable from year to year, spatial distribution of yield is the result of the interaction between the soil characteristics, position in the landscape and weather (i.e. the

performance of an unstable area of the field will have stronger variation compared to the rest of the field depending on the year's weather).

In this study, we examined the correlation between yield and 4 covariates, three were derived from remote sensing imagery (red band spectral reflectance, NDVI and surface temperature) and the fourth entailed the use of yield maps from previous years. Each of these covariates is well-correlated to yield for various reasons. The red band reflects the amount of light that is not absorbed by the plant in the red portion of the electromagnetic spectrum and is therefore negatively correlated with the photosynthesis. In a similar fashion, NDVI (Tucker, 1979) represents the normalized difference between the near infrared (emitted by leaves) and red (absorbed by leaves) and is positively correlated to plant photosynthetic activity. Surface temperature is a proxy for plant transpiration and thus, soil water availability and plant photosynthetic rate.

We investigated the above-mentioned four covariates using a dataset that encompasses fields from eight states of the Midwest of the United States cultivated with maize (*Zea mays* L.), wheat (*Triticum*

* Corresponding author.

E-mail address: basso@msu.edu (B. Basso).

spp.L.), soybean (*Glycine max*, L.) and cotton (*Gossypium* spp. L.).

We investigated the following research questions: 1) In what part of the growing season is the correlation between crop growth and plant spectral reflectance the highest in our 571 fields? We hypothesize that the best correlation for maize occurs in July, as reported by Johnson (2014) at the county level, because the processes governing the correlation (photosynthesis level) are the same at the two spatial scales (field and county); 2) Is the correlation between within-season images and yield stronger than the correlation between past yield maps and yield? We hypothesized that historical yield maps exhibit a stronger correlation because they are a proxy for the interaction between soil conditions and past weather along with crop phenology, whereas the individual within-season images reflect the effects of the weather on growth only at the time of the image (single crop stage).

To test our hypothesis under the most rigorous conditions, we compared the variable importance of the historical yield against the post-facto NDVI images (i.e. the NDVI image that showed the best correlation with the yield at harvest, although clearly in reality it is not possible to know beforehand which will be the within-season image that exhibit the best correlation). We further hypothesized that historical yield is the best predictor only in the stable zones whereas unstable zones have by definition poor correlation with the yield of previous years and therefore they can be better predicted using within season remotely sensed images.

2. Materials and methods

2.1. Yield data

We collected yield maps from 571 fields from 110 farmers, for a total number of 2009 fields-year maps. In 27% of the fields we had more than 4 years of yield maps. The fields were in 8 different states of the Midwest of the United States, as shown in Map 1. The distribution of the yields collected for each field and the number of yield maps collected for each state in shown in the Table SI 1.

For each harvest point dataset (i.e. the points recorded by the harvester monitoring system relative to one year), the median was used to define the lower ($0.1 \times$ median) and higher ($3 \times$ median) boundaries. All points below or above the boundaries were handled as outliers and deleted. Points with the same longitude and latitude were dissolved to avoid duplicates. The average minimum distance between points was 1.3 m with an average standard deviation between fields of 0.6 m and within field of 0.4 m. We applied to each harvest point dataset a spherical kriging model with a cell size of 2 by 2 m, and a fixed radius with a distance of 20 m and a minimum of 12 points to rasterize the point dataset.

For every field, we calculated the border of polygon representing the field, and removed the yield maps that covered less than 75% of the field. We calculated field boundaries first by merging all the georeferenced points into a unique dataset and then by creating a polygon around the points based on an aggregation distance varying depending on the number of years of harvest available. The aggregation distance was set to 15 m (3 or more years of yield data), 20 m (2 years of yield data) or 30 m (1 year of yield data). For each field, we resampled the yield maps to have all the same spatial extent to allow a pixel wise analysis using bilinear interpolation. Additionally, we removed the years for which more than one yield map for the same field was available because in those years there were two different crops cultivated in different sections of the field. Fig. 1 shows the geographical distribution of the fields.

2.2. Red band from aerial visual images

Visual imagery for 121 fields was collected in the red, green and blue bands (RGB) by Airscout, a commercial airborne image company operating in the Midwest US. Of the total number of fields, images were

collected of 93 fields for one year, 25 fields for two years, and one field for 3 years. We only considered the red band, as this is a proxy of the light absorbed by plants. Images were taken between the 4th of April and the 10th of October (Fig. SI 2a) in 2014 (3 fields), 2015 (39 fields) and 2016 (102 fields). The flights hours were uniformly distributed between 9 a.m. and 6 p.m. (Fig. SI 2b). The resolution of the red band images was on average 0.30 m (sd 0.05), the resolution varied depending on the flying height of the airplane (Fig. SI 2c). In the few cases where multiple pictures of a field were taken at interval lower than one hour, raster images were averaged, under the assumption that either multiple pictures were taken by mistake or that each picture represents only a portion of the field. Raster images were resampled (using a bilinear interpolation method) and projected to match the resolution and projection of the yield maps.

2.3. Airborne plant temperature and visual images

Plant surface temperature and visual (RGB) images were taken simultaneously from 130 fields, in 9 fields the temperature image was available whereas the red band image was not available. The resolution of the temperature images was on average 2.2 m (sd 0.2, Fig. SI 3c). We resampled the temperature images to match the yield maps resolution, extent, and projection. This operation was necessary to perform a pixel-wise analysis of the correlation between the temperature image and yield image. The resampling method adopted was a bilinear interpolation method. As for the images of the red band reflectance, in the few cases where multiple pictures of the field were taken at a time distance lower than one hour the raster images were averaged, under the assumption that either multiple pictures were taken by mistake or that each picture represents only a portion of the field. We removed pixels indicating temperature values higher than 50 °C as they may indicate a measurement error.

2.4. Landsat 8 derived NDVI images

We downloaded all the images available for each field from April 1, 2014–November 1, 2016 using the python package *Landsat-util*. We screened all the images to mark as not available (NA) those pixels whose quality was affected by clouds, points that contained designated fills and dropped frames using the Landsat 8 Pre-Collection Quality Assessment. We then removed the images for which more than 25% of pixels in the field were marked as not available. We calculated the NDVI for each Landsat scene using the following formula:

$$NDVI = \frac{NIR - RED}{NIR + RED}$$

We report the distribution of the number of images available in the period July–August in the Fig. SI 4, the median of the distribution is 3. To measure the correlation between yield maps and NDVI images, we resampled the yield maps to match the resolution of the Landsat images using the bilinear interpolation method.

2.5. Historical yield

For the fields for which we had yield maps from at least four years, we calculated a *historical yield map* using the following algorithm: first, we normalized each yield map (i.e. centered and scaled to have mean = 0 and sd = 1); second, for each year we calculated the pixel-wise mean of the previous years' normalized yield maps. We calculated the historical yield map only for those years where at least three previous yield maps were available. For example, if there were yield maps for 2012, 2013, 2014 and 2015 for a field, the historical map was calculated only for 2015, whereas if there were yield maps only for 2013, 2014, and 2015, no historical map was calculated for that field. Conversely, if yield maps for 2012–2016 were available, we calculated the historical map for both 2015 and 2016. We used only maps from the

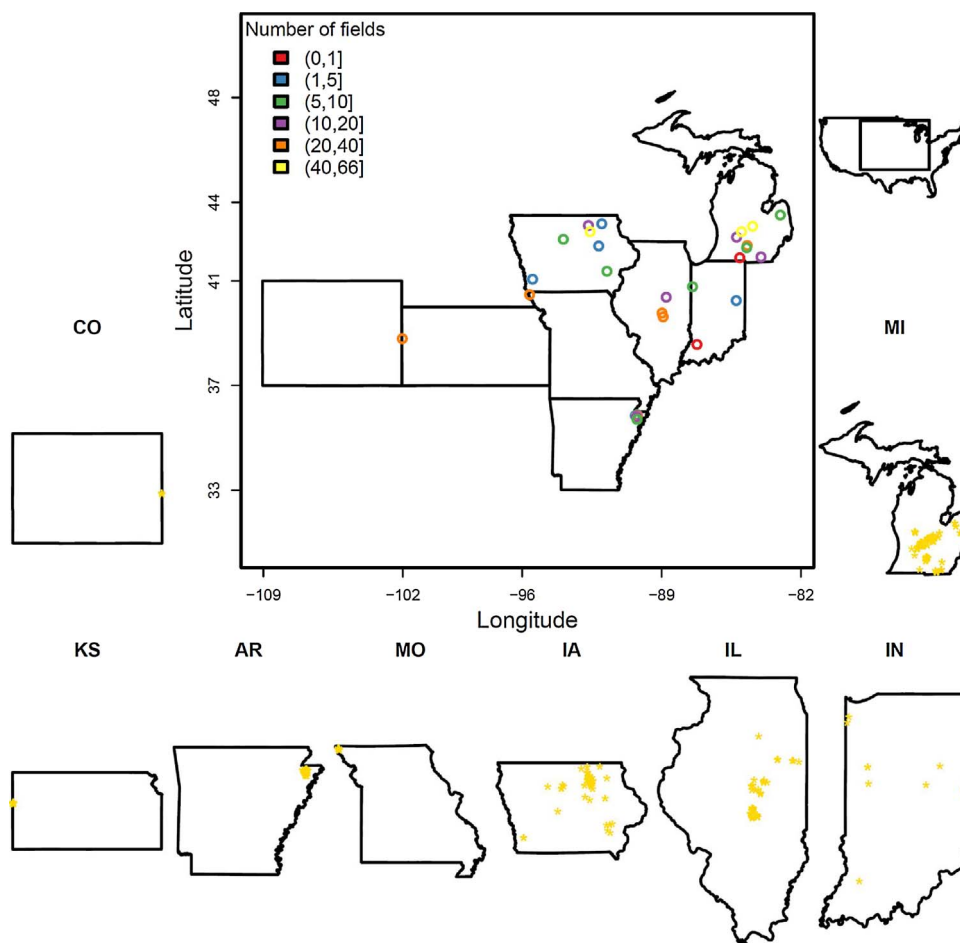


Fig. 1. Geographical distribution of the fields in the considered in the present study. The color of the circles reflects the number of fields in the area. The stars within each state map indicate the location of individual fields.

previous years to simulate the real conditions of the farmer who obviously do not have the yield maps of future years. We calculated at least one historical map for 265 fields.

2.6. Yield stability maps

For the 339 fields for which at least three years of yield maps were available, we calculated a stability map using the following algorithm: first, we normalized each yield map (i.e. centered and scaled to mean = 0 and sd = 1); second, we calculated for every pixel the standard deviation of all yield maps recorded; third, we set as unstable the pixels that had standard deviation larger than the 80th percentile of the map of the standard deviation of the yield. Therefore, in each field 20% of the pixels were categorized as unstable and 80% were categorized as stable.

2.7. Statistical method

For our first hypothesis (correlation of yield and within season images across the season) the response variable representing the subject of the analysis was the correlation between yield and a set of covariates (NDVI, temperature, red band, historical yield map).

We calculated the correlation between the yield and each of the covariates using the Spearman rank correlation coefficient at within field level. The Spearman rank correlation is equal to the Pearson correlation coefficient applied to the ranks of the variables:

$$r = \frac{cov(x, y)}{sd(x)*sd(y)}$$

Where $cov(x,y)$, where cov indicate the covariance between the ranks of yield and the second variable and sd of their ranks. The Spearman rank correlation was used instead Pearson correlation as within-field yield data are negatively skewed and broader than a normal distribution (Joernsgaard and Halmoe, 2003).

We then transformed the correlation coefficient (r) using the Fisher’s z transformation in order to transform the Pearson correlation coefficient into a new variable whose domain is the set of real numbers (i.e. is no longer bounded between -1 and 1 , like the correlation coefficient but between $-\infty$ and $+\infty$).

The Fisher’s Z transformation function is the following:

$$z = 0.5*ln(1 + r) - ln(1 - r)$$

We tested the null hypothesis that there was no significant difference between the correlation covariate-yield for images taken at different time of the growing season (May–October). We created for each of the remote sensing predictor (NDVI, red band, and surface temperature) and crop a dataset that included the available images for that predictor (resampled to match the yield) and the yield measured at the end of the season. We tested the null hypothesis (the correlation between yield and the covariate does not change during the growing season) using a linear mixed model, with nested random effects. Random effects were the state, the farmer and the field identifier. The model equation that was fit to each dataset was the following:

$$Fz(r) = \alpha + \beta*DOY_{cat} + \epsilon_{state} + \epsilon_{farmer} + \epsilon_{field} + \epsilon_{residuals}$$

Where the $Fz(r)$ is the spearman correlation coefficient transformed using Fisher’s transformation, DOY_{cat} is the day of the year binned in groups of 15 days, and β is the vector of estimated coefficients

Table 1
Models fitted to the different datasets. The column indicate the crops analyzed in the subset, the stability of the points included in the subset, the model selected using the AICc criterion, the estimated model parameters, the number of fields-year in the dataset and the number of fields, ϵ_1 and ϵ_2 are the standard deviation of the random effect normally distributed as $N(0, \epsilon)$ whose levels are the fields-year combinations whereas ϵ_{res} is the standard deviation of the residuals.

Crop	Dataset	Most important variable	A	β	ϵ_1	ϵ_2	ϵ_{res}	AICc (k)	N. fields-year	N. fields	Model equation
a)											
Maize	Stable and Unstable	historic avg.	9.95 (0.15)	1.05 (0.04)	1.98	0.52	1.0	195.3	183	145	Yield = $\alpha + \epsilon_1 + (\beta + \epsilon_2) \times \text{historic avg.} + \epsilon_{res}$
			-2.8 (0.8)	25.5 (1.5)	10.7	20.6	1.1	200.9	183	145	Yield = $\alpha + \epsilon_1 + (\beta + \epsilon_2) \times \text{post-facto best NDVI} + \epsilon_{res}$
Cotton	Unstable and Stable	historic avg.	3.46 (0.07)	0.28 (0.03)	0.47	0.17	0.36	9.7	40	33	Yield = $\alpha + \epsilon_1 + (\beta + \epsilon_2) \times \text{historic avg.} + \epsilon_{res}$
			0.6 (0.2)	5.8 (0.5)	1.2	2.8	0.36	9.8	40	33	Yield = $\alpha + \epsilon_1 + (\beta + \epsilon_2) \times \text{post-facto best NDVI} + \epsilon_{res}$
Soybean	Stable and Unstable	post-facto best NDVI	3.68 (0.05)	0.38 (0.02)	0.75	0.21	0.49	624.9	199	183	Yield = $\alpha + \epsilon_1 + (\beta + \epsilon_2) \times \text{post-facto best NDVI} + \epsilon_{res}$
			-0.7 (0.2)	8.1 (0.3)	2.7	4.7	0.46	556.2	199	183	Yield = $\alpha + \epsilon_1 + (\beta + \epsilon_2) \times \text{historic avg.} + \epsilon_{res}$
Wheat	Unstable and Stable	historic avg.	6.26 (0.23)	0.72 (0.06)	1.31	0.35	0.72	24.3	32	32	Yield = $\alpha + \epsilon_1 + (\beta + \epsilon_2) \times \text{post-facto best NDVI} + \epsilon_{res}$
			2.8 (0.8)	6.7 (2.4)	4.6	13.3	0.82	27.2	32	32	Yield = $\alpha + \epsilon_1 + (\beta + \epsilon_2) \times \text{historic avg.} + \epsilon_{res}$
b)											
Maize	Stable	historic avg.	9.99 (0.15)	1.08 (0.04)	2.00	0.47	0.8	130.6	183	145	Yield = $\alpha + \epsilon_1 + (\beta + \epsilon_2) \times \text{post-facto best NDVI} + \epsilon_{res}$
			-1.8 (0.8)	23.6 (1.5)	10.5	20.0	0.9	142.3	183	145	Yield = $\alpha + \epsilon_1 + (\beta + \epsilon_2) \times \text{historic avg.} + \epsilon_{res}$
Cotton	Stable	historic avg.	3.44 (0.07)	0.34 (0.03)	0.47	0.16	0.26	2.1	40	33	Yield = $\alpha + \epsilon_1 + (\beta + \epsilon_2) \times \text{post-facto best NDVI} + \epsilon_{res}$
			0.3 (0.2)	6.4 (0.5)	1.3	2.8	0.3	4.3	40	33	Yield = $\alpha + \epsilon_1 + (\beta + \epsilon_2) \times \text{historic avg.} + \epsilon_{res}$
Soybean	Stable	historic avg.	3.70 (0.05)	0.41 (0.01)	0.75	0.20	0.37	305.8	199	183	Yield = $\alpha + \epsilon_1 + (\beta + \epsilon_2) \times \text{post-facto best NDVI} + \epsilon_{res}$
			-0.8 (0.2)	8.1 (0.4)	2.8	5.0	0.39	336.2	199	183	Yield = $\alpha + \epsilon_1 + (\beta + \epsilon_2) \times \text{historic avg.} + \epsilon_{res}$
Wheat	Stable	historic avg.	6.26 (0.23)	0.76 (0.07)	1.30	0.39	0.58	15.8	32	32	Yield = $\alpha + \epsilon_1 + (\beta + \epsilon_2) \times \text{post-facto best NDVI} + \epsilon_{res}$
			2.8 (0.8)	6.5 (2.2)	4.7	12.4	0.69	19.0	32	32	Yield = $\alpha + \epsilon_1 + (\beta + \epsilon_2) \times \text{historic avg.} + \epsilon_{res}$
Maize	Unstable	post-facto best NDVI	9.81 (0.15)	0.93 (0.05)	1.97	0.66	1.6	50.3	183	145	Yield = $\alpha + \epsilon_1 + (\beta + \epsilon_2) \times \text{post-facto best NDVI} + \epsilon_{res}$
			-2.7 (0.8)	24.9 (1.5)	9.8	18.8	1.5	49.6	183	145	Yield = $\alpha + \epsilon_1 + (\beta + \epsilon_2) \times \text{historic avg.} + \epsilon_{res}$
Cotton	Unstable	post-facto best NDVI	3.45 (0.08)	0.17 (0.04)	0.49	0.22	0.55	4.1	40	33	Yield = $\alpha + \epsilon_1 + (\beta + \epsilon_2) \times \text{post-facto best NDVI} + \epsilon_{res}$
			1.1 (0.3)	4.8 (0.5)	1.4	3.0	0.52	3.8	40	33	Yield = $\alpha + \epsilon_1 + (\beta + \epsilon_2) \times \text{historic avg.} + \epsilon_{res}$
Soybean	Unstable	post-facto best NDVI	3.58 (0.06)	0.25 (0.02)	0.80	0.29	0.78	205.2	199	183	Yield = $\alpha + \epsilon_1 + (\beta + \epsilon_2) \times \text{post-facto best NDVI} + \epsilon_{res}$
			-0.3 (0.2)	7.1 (0.4)	2.8	4.6	0.65	172.9	199	183	Yield = $\alpha + \epsilon_1 + (\beta + \epsilon_2) \times \text{historic avg.} + \epsilon_{res}$
Wheat	Unstable	historic avg.	6.15 (0.24)	0.59 (0.07)	1.35	0.37	1.1	6.8	32	32	Yield = $\alpha + \epsilon_1 + (\beta + \epsilon_2) \times \text{post-facto best NDVI} + \epsilon_{res}$
			2.6 (0.9)	6.2 (2.2)	4.6	12.0	1.1	7.0	32	32	Yield = $\alpha + \epsilon_1 + (\beta + \epsilon_2) \times \text{historic avg.} + \epsilon_{res}$

associated to each *DOYcat*. The terms ε_{state} , ε_{farmer} , ε_{field} where are random effect of the intercept associated respectively to the state, the farmer and field, whereas $\varepsilon_{residuals}$ indicate the residuals.

To investigate whether historical yield is a better predictor of spatial yield distribution than remote sensing images, we compared two simple models: in the first model the explanatory variable was the historical yield whereas in the second model the explanatory variable was the best post-facto NDVI image. In each model, we also included two random effects, one random effect of the intercept and one random effect of the slope. In both cases the levels of the random effect were accounted for each field-year combination. We report model formulas in Table 1.

To select the best model, we used the Second-Order Information Criterion (AICc, Sugiura, 1978), where the penalty term was adjusted to account for pseudo-replication as suggested in Burnham (2002). We used as sample size to estimate the penalization the number fields-year in the dataset, we calculated the AICc using the following formula:

$$AICc = -2 \times \log Likelihood(\hat{\theta}) + 2 \times K \times \frac{n}{n - k - 1}$$

To compare the use of within-season images with the historical yield, we chose to focus solely on the NDVI index rather than surface temperature images and red band images, because as observed in Fig. 1 the NDVI images had a higher correlation than the surface temperature images and the red band images. We compared the two models separately first on each crop for the whole field and then for each crop first only in the stable portions of the field and then only in the unstable portion of the fields.

- 1) We identified for each field-year the NDVI image that had the best spearman correlation with the yield measured at the end of the season. As noted in the introduction this is a post-facto analysis, however we opted to choose the image with the best correlation in order to verify our hypothesis under more rigorous conditions.
- 2) We resampled each yield image and previous harvest image to match the resolution and spatial extent of the NDVI images.
- 3) We created a dataset composed of all the pixels in the dataset with the following columns: final yield (response variable), NDVI (explanatory variable), historical yield average (explanatory variable), crop and field identifier.
- 4) We removed from the dataset the rows (i.e. the pixels) where at least one variable was missing. This step was necessary to ensure that model likelihood was calculated on the same dataset for each model.
- 5) We split the dataset by crop first (Table 1a) and by crop and then by crop and stability (Table 1b) and fit the two models to each subset and selected the best model based on the AICc.

To better visualize the performance of the different predictors, we calculated for each remote-sensing predictor the average spearman correlation between yield and the best post-facto image separately for the stable and unstable portions of the field (Fig. 3).

The statistics were calculated using R v 3.2.3 and the R libraries *raster* (Hijmans, 2016) for raster manipulation, *lme4* (Bates et al., 2015) to fit mixed models, *snow and snowfall* (Tierney et al., 2016) for parallel computing.

3. Results

3.1. Research question 1

For Maize, the best correlation between NDVI maps derived from Landsat images and yield maps occurred between the last week of July and the first week of August (Figs. 2 and S5, $p < 0.05$). For wheat, soybean and cotton, we did not identify a single 15-day interval that exhibited the best correlation between NDVI and yield across all the fields analyzed (Figs. 2 and S5). The correlation between yield and the

other remote sensing variables (temperature, red band) did not show a hump shape with a clear period having a stronger correlation than the others (Figs. 2 and S5).

3.2. Research question 2

We found that when we considered the whole field (i.e. both stable plus unstable portions) the model including the historical yield was the best predictor according to the AICc criterion for maize, wheat and cotton, but not for soybean (Table 1).

When the analysis was limited to the stable zones we found that the model including the average correlation between historical yield average and yield was better than the average correlation observed between the “best” image and the yield for all the type of remote sensing images analyzed here (Fig. 3). The model selection procedure confirmed it (Table 1b) by showing that the best model to predict the yield in the stable portions of the fields was the historical yield for all the crops.

In the unstable portions of the fields the historical yield was a poor predictor of the yield spatial distribution, whereas the images derived from remote sensing didn't show a difference between their correlation with yield in stable and unstable zones and NDVI exhibited the best correlation with yield in the unstable zones. The model selection procedure confirmed the better performance of NDVI images in unstable zones for all crops except wheat.

4. Discussion

4.1. Temporal variability and signs of the correlation coefficients

The NDVI was positively correlated with yield as it is an indicator of canopy size and thus photosynthetic activity. The red band was negatively correlated with yield. Higher reflectance in the red band indicates presences of other compounds such as carotenoid, xanthophyll that mask green chlorophyll molecules, lowering plant photosynthesis. Temperature, as expected, was also negatively correlated with the yield because it is an indicator of plant being hot and not being able to transpire at the evaporative demand rate. A plant that is photosynthetically active will have open stomata resulting in higher transpiration when water is available which in turn, reduces canopy surface temperature. In the early stages of plant development other processes that are independent from the plant growth and thus from the yield are strongly influencing the surface temperature. For example, in the early phenological stages, corresponding to relatively little ground cover, the surface temperature is mostly controlled by physical processes occurring in the soil like fluxes of latent heat flux due to water evaporation (Fengshan et al., 2017). Surface temperature correlated negatively with yield in the July-August period, confirming at subfield level the findings for maize by Johnson (2014) at the county level. Similarly, plants with lower reflectance in the red band are characterized by lower amounts of orange-red pigments (carotenoid, xanthophyll) and healthier conditions. Our findings confirm both these theories, however the correlation of both the red band and temperature with yield, even though existed, was weaker than the correlation obtained using the NDVI index (Fig. 2).

We showed that images of maize between the end of July and the beginning of August exhibit the strongest correlation between yield and the NDVI index, such consistency across eight different states is surprising considering the differences that exist regarding the sowing dates and the climates. With regard to corn and soybean, our findings measured at the sub-field level agree with the data measured at the county level by Johnson, (2014). This suggests that this correlation holds at multiple scales (county level and within field).

4.2. Management strategies for the stable and unstable zones

Using model selection and averaged correlation coefficients, we

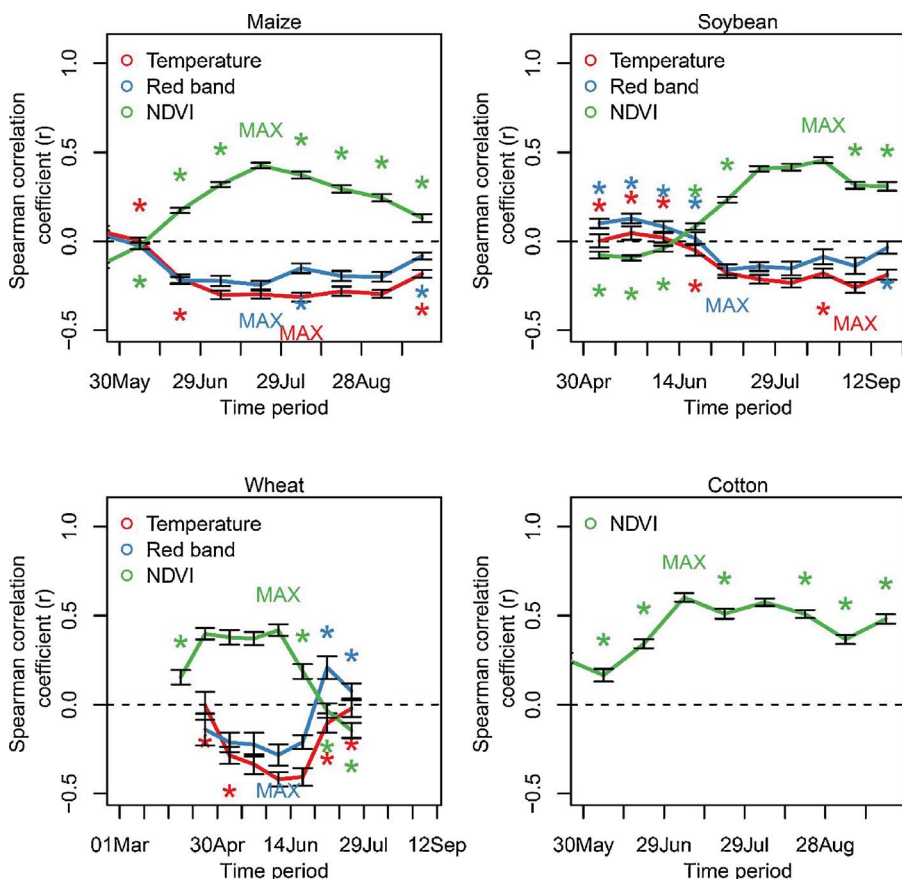


Fig. 2. Trend over time of the correlation coefficients (r) between yield and airborne-derived covariates collected with from an airplane (red band and temperature) and satellite images (NDVI), divided by crops. The time has been grouped in periods of 15 days, the label “MAX” on top of the curve indicate the time of the year when the spatial correlation between yield and the covariate of interest was stronger and it was calculated as the absolute value of r. The stars indicate the dates that were significantly different from the date that exhibits the maximum correlation. The significance of the difference between the maximum date and the other was calculated using a mixed model, where the time period with maximum correlation was set as the intercept. The estimates of the coefficients of the models employed is reported in Fig. SI 4. The error bars represent the standard error of the mean. (For interpretation of the references to colour in this figure legend, the reader is referred to the web version of this article.)

observed that the most important predictor of yield distribution in stable zones is the historical yield, whereas in unstable zones yield spatial distribution are more correlated to within-season images.

This finding implies that in zones that are stable, the spatial distribution of yield is less dependent on the year’s weather. Despite favorable or unfavorable weather that they may receive a point that has on average high yields and that is stable will always be high compared to the rest of the field. We hypothesize that the relative yield in unstable zones depends on weather conditions and therefore vary from year to year. For example, it is possible that unstable zones are concave areas that are waterlogged in wet years and relatively more humid in dry years, resulting in high oscillation of the yield.

This has important management implications. In fact, the stable zones may be managed using a zone-specific management strategy —

selected before the season, often called strategic (Basso et al., 2011) — obtained from running crop models with site-specific input and calibrated over a long-time weather and yield records. Once the different management scenarios and the associated uncertainty are available, the farmer implements the most sustainable management practice from the economic and environmental standpoint (tradeoff between net revenue and environmental outcomes like nitrate leaching) (Basso et al., 2011). For instance, if a validated crop model indicates that in 24 out of 30 years of observed weather a fertilization rate of 150 kg N/ha gives the same yield of 200 kg N/ha, the farmers may choose to apply 150 kg N/ha knowing that there is a 20% possibility (6 years out of 30) that applying a higher fertilization rate would have resulted in a higher yield. In unstable zones, the adoption of a zone-specific management strategy before the season may not be sufficient to match supply and

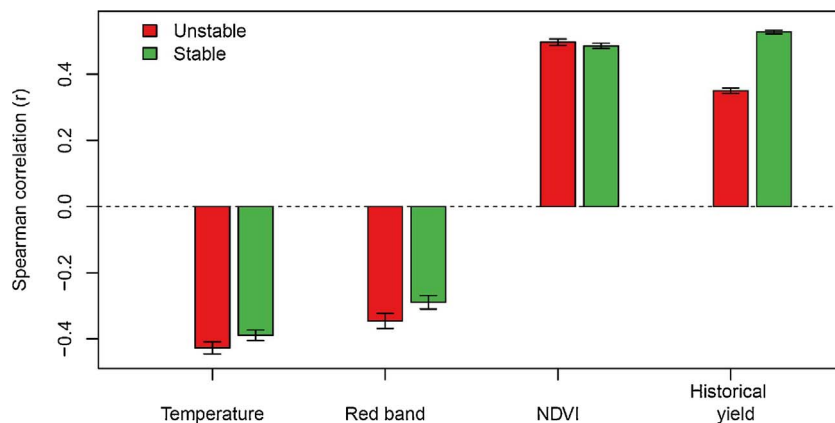


Fig. 3. Average correlation between covariates and yield. The red bar represents the correlation coefficient calculated only on the portion of the field defined as unstable and the green bar only on the portion of the field defined as stable. (For interpretation of the references to colour in this figure legend, the reader is referred to the web version of this article.)

demand, and within-season adjustment to the management strategy may be necessary depending on the interaction between the observed weather and crop response, since the response in unstable zones is strictly dependent of weather. This approach is often called tactical (Basso et al., 2011). For example if the weather forecasts are favorable the farmer chooses the before-season management scenarios obtained from running the models under favorable scenarios, whereas if the year is characterized by unfavorable conditions, then the best management strategies will be chosen from years that better reflect these conditions. Using this approach the use of remote sensing in the management of unstable zones starts when the first within-season images are available and can be used to match up supply and demand considering not just nitrogen availability, but also the amount of soil water available to plants to efficiently use the available nitrogen. (Basso et al., 2011, 2007; Dumont et al., 2015).

A challenge in the management of unstable zones is that the predictors of spatial variability may be available only when a limited set of options for management are available to the farmer. However, more farmers are becoming equipped with high-wheels fertilizer spreader to apply N fertilizer later in the season in amounts that would vary over space and depending on the weather received that season. Another important aspect to consider, though, is still the knowledge of yield before the end of the season to better refine sale and storage of the products to be harvested.

4.3. Historical yield was the best predictor for the spatial distribution of the yield

When we considered the field as a whole (i.e. without partitioning between stable and unstable portions), the model having as predictor the yield of the previous years were better than models having as predictor the best image in the season, for all the crops but soybean. However, it is important to consider that we gave to the NDVI images the advantage of choosing among the images in the season the image that showed the best correlation with the yield, a situation that clearly is not happening in reality where NDVI images are usually used to predict future yields.

One possible explanation for the lower performance of individual images compared to the historical yield is that they are connected only to one phase of the plants. The historical yield will represent a spatial index that is a combination of all the processes that regulate the yield, in corn for example kernel development and filling. On the contrary, airborne images will only capture one individual stage of the development at a time, therefore while individual images may be of little help if used to predict the yield spatial distribution they could be of great if used to calibrate crop models coupled to land surface models. For example by coupling land surface models and crop models it would be possible to obtain surface heat as a model output and use it to calibrate the model within the growing season and simulate the effect of the different management options. However although several attempts have been done to couple crop phenology and land surface models their use is still mostly limited to simulate the effect of changes in crop management on land surface processes (e.g. Sacks and Kucharik, 2011; Song et al., 2013) whereas the use of coupled models to improve the accuracy of crop models need further research.

5. Conclusion

This study is the first research to report a Big-Data approach (571 fields for multiple years) on the within field correlation between different covariates (Landsat-derived NDVI, red band at 0.3 m resolution

and temperature at 2 m resolution). Our findings have two important management implications: first it validates the management by yield approach, where the management follows the principle that the inputs should reflect to the potential of the areas. This approach may prove particularly valid for the stable zones if coupled to modeled yield predictions based on weather forecast. Secondly that the use of satellite images may be a valuable tool to inform within-season decisions for the unstable zones, like the late application of N using new high-wheels fertilizer spreaders.

Acknowledgments

This research has been supported by USDA/NIFA under awards 2015-68007-23133, the Swiss National Science Foundation (project number 167689); U.S. National Science Foundation's Dynamics of Coupled Natural and Human Systems Program (award 1313677), Michigan Corn Marketing Program, Michigan Wheat Program, and Michigan State University AgBioResearch and USDA/NIFA HATCH grant N. MCL02368.

Appendix A. Supplementary data

Supplementary data associated with this article can be found, in the online version, at <https://doi.org/10.1016/j.fcr.2018.01.028>.

References

- Basso, B., Bertocco, M., Sartori, L., Martin, E.C., 2007. Analyzing the effects of climate variability on spatial pattern of yield in a maize-wheat-soybean rotation. *Eur. J. Agron.* 26, 82–91. <http://dx.doi.org/10.1016/j.eja.2006.08.008>.
- Basso, B., Ritchie, J.T., Cammarano, D., Sartori, L., 2011. A strategic and tactical management approach to select optimal N fertilizer rates for wheat in a spatially variable field. *Eur. J. Agron.* 35, 215–222. <http://dx.doi.org/10.1016/j.eja.2011.06.004>.
- Bates, D., Maechler, M., Bolker, B., Walker, S., 2015. *lme4: Linear Mixed-effects Models Using Eigen and S4*.
- Blackmore, S., 2000. The interpretation of trends from multiple yield maps. *Comput. Electron. Agric.* 26, 37–51. [http://dx.doi.org/10.1016/S0168-1699\(99\)00075-7](http://dx.doi.org/10.1016/S0168-1699(99)00075-7).
- Burnham, Kenneth P., 2002. *Model Selection and Multimodel Inference: a Practical Information-theoretic Approach*, 2nd ed. Springer-Verlag, New York.
- Dumont, B., Basso, B., Leemans, V., Bodson, B., Destain, J.P., Destain, M.F., 2015. Systematic analysis of site-specific yield distributions resulting from nitrogen management and climatic variability interactions. *Precis. Agric.* 16, 361–384. <http://dx.doi.org/10.1007/s11119-014-9380-7>.
- Fengshan, L., Ying, C., Wenjiao, S., Shuai, Z., Fulu, T., Quansheng, G., 2017. Influences of agricultural phenology dynamic on land surface biophysical process and climate feedback. *J. Geogr. Sci.* 27 (9), 1085–1099.
- Hijmans, R.J., 2016. raster: Geographic Data Analysis and Modeling.
- Joergsgaard, B., Halmoe, S., 2003. Intra-field yield variation over crops and years. *Eur. J. Agron.* 19, 23–33. [http://dx.doi.org/10.1016/S1161-0301\(02\)00016-3](http://dx.doi.org/10.1016/S1161-0301(02)00016-3).
- Johnson, D.M., 2014. An assessment of pre- and within-season remotely sensed variables for forecasting corn and soybean yields in the United States. *Remote Sens. Environ.* 141, 116–128. <http://dx.doi.org/10.1016/j.rse.2013.10.027>.
- Koshla, R., Westfall, D.G., Reich, R.M., Mashal, J.S., Gangloff, W.J., 2010. Spatial variation and site-specific management zones. In: Oliver, M.A. (Ed.), *Geostatistical Applications for Precision Agriculture*. Springer Netherlands, Dordrecht, pp. 195–219.
- Sacks, W.J., Kucharik, C.J., 2011. Crop management and phenology trends in the US Corn Belt: impacts on yields, evapotranspiration and energy balance. *Agric. For. Meteorol.* 151 (7), 882–894.
- Schepers, A.R., Shanahan, J.F., Liebig, M.A., Schepers, J.S., Johnson, S.H., Luchiar, A., 2004. Appropriateness of management zones for characterizing spatial variability of soil properties and irrigated corn yields across years. *Agron. J.* 96, 195–203. <http://dx.doi.org/10.2134/agronj2004.0195>.
- Song, Y., Jain, A.K., McIsaac, G.F., 2013. Implementation of dynamic crop growth processes into a land surface model: evaluation of energy, water and carbon fluxes under corn and soybean rotation. *Biogeosciences* 10 (12) 8201–8201.
- Sugiura, N., 1978. Further analysis of the data by Akaike's information criterion and the finite corrections. *Commun. Stat. A* 7, 13–26.
- Tierney, L., Rossini, A.J., Li, N., Sevcikova, H., 2016. snow: Simple Network of Workstations.
- Tucker, C., 1979. Red and photographic infrared linear combinations for monitoring vegetation. *Remote Sens. Environ.* 8 (150), 127–150.